



# Colony stimulating factor I receptor inhibition eliminates microglia and attenuates brain injury after intracerebral hemorrhage

Minshu Li<sup>1,2,\*</sup>, Zhiguo Li<sup>2,\*</sup>, Honglei Ren<sup>1</sup>,  
Wei-Na Jin<sup>1,2</sup>, Kristofer Wood<sup>2</sup>, Qiang Liu<sup>1,2</sup>,  
Kevin N Sheth<sup>3</sup> and Fu-Dong Shi<sup>1,2</sup>

## Abstract

Microglia are the first responders to intracerebral hemorrhage, but their precise role in intracerebral hemorrhage remains to be defined. Microglia are the only type of brain cells expressing the colony-stimulating factor I receptor, a key regulator for myeloid lineage cells. Here, we determined the effects of a colony-stimulating factor I receptor inhibitor (PLX3397) on microglia and the outcome in the context of experimental mouse intracerebral hemorrhage. We show that PLX3397 effectively depleted microglia, and the depletion of microglia was sustained after intracerebral hemorrhage. Importantly, colony-stimulating factor I receptor inhibition attenuated neurodeficits and brain edema in two experimental models of intracerebral hemorrhage induced by injection of collagenase or autologous blood. The benefit of colony-stimulating factor I receptor inhibition was associated with reduced leukocyte infiltration in the brain and improved blood–brain barrier integrity after intracerebral hemorrhage, and each observation was independent of lesion size or hematoma volume. These results demonstrate that suppression of colony-stimulating factor I receptor signaling ablates microglia and confers protection after intracerebral hemorrhage.

## Keywords

Colony stimulating factor I receptor inhibitor; intracerebral hemorrhage, brain edema, microglia, inflammation

Received 15 May 2016; Revised 29 July 2016; Accepted 4 August 2016

## Introduction

Intracerebral hemorrhage (ICH) is an important public health problem with high rates of mortality and disability. The focus of many therapeutic interventions to date has been toward the prevention of hematoma expansion. Hemostatic and antihypertensive therapies are two such interventions, but thus far, those efforts have not reduced hematoma expansion or improved outcomes.<sup>1</sup> Emerging results show that the inflammatory cascade accelerates the formation of edema that surrounds hematomas, exacerbates the mass effect, and amplifies the cell death process.<sup>2–6</sup> As resident cells in the brain, microglia are the first responders to ICH and engage in intimate cross-talk with other intrinsic brain cells and infiltrating leukocytes that enter the brain from the periphery through the compromised blood–brain barrier (BBB).<sup>3,7,8</sup> Following ICH, microglia acquire properties of antigen presentation, reactive species generation,

phagocytosis, and the production of inflammatory mediators including matrix metalloproteinase (MMP), tumor necrosis factor- $\alpha$  (TNF- $\alpha$ ), interleukin-1 beta (IL-1 $\beta$ ), and interleukin-6 (IL-6).<sup>8–12</sup> Of note, microglia also possess an anti-inflammatory role by secreting factors such as interleukin-4 (IL-4) and interleukin-10 (IL-10) during the resolution and repair processes, upon returning to a

<sup>1</sup>Department of Neurology, Tianjin Neurological Institute, Tianjin Medical University General Hospital, Tianjin, China

<sup>2</sup>Department of Neurology, Barrow Neurological Institute, St. Joseph's Hospital and Medical Center, Phoenix, USA

<sup>3</sup>Department of Neurology, Yale University School of Medicine, New Haven, USA

\*These authors contributed equally to this work.

## Corresponding author:

Fu-Dong Shi, Department of Neurology, Tianjin Neurological Institute, Tianjin Medical University General Hospital, Tianjin 300052, China.  
Email: fshi@tmu.edu.cn

surveillance state.<sup>13,14</sup> These features imply that microglia would be active players during hematoma expansion and secondary brain injury. However, the impact of microglia on the outcome of ICH remains unclear.

The survival of microglia depends on colony stimulating factor 1 receptor (CSF1R) signaling.<sup>15,16</sup> CSF1R is expressed by myeloid lineage cells including macrophages, microglia, and osteoclasts.<sup>17</sup> In the brain, microglia are the only cell type that expresses CSF1R under physiological conditions.<sup>18,19</sup> Of note, CSF1R knockout mice are born without microglia and mice lacking either of its two ligands, CSF1 or IL-34, also have reduced microglial numbers.<sup>18,20,21</sup> It has also been demonstrated that treatment of adult mice with PLX3397 for 21 days, a CSF1R inhibitor, leads to nearly complete elimination of 99% of all microglia from the adult central nervous system (CNS) and reduces lipopolysaccharide (LPS) neuroinflammation, but does not affect cognition or behavior.<sup>15,22</sup> Moreover, microglia elimination persists throughout the entire period of treatment, allowing for indefinite microglial elimination from the adult brain.<sup>15</sup> Therefore, CSF1R inhibition offers an opportunity to investigate the pathogenesis of ICH in relation to microglia. In this study, we adopted two models for ICH by injection of collagenase or autologous blood to mice, respectively. We administered PLX3397 to ICH mice and quantified neurological function and brain pathology. Our results show that CSF1R inhibition eliminates microglia and confers protection after ICH.

## Materials and methods

### Human brain specimens

Human brain sections were obtained from Tianjin General Hospital (Tianjin, China) and Barrow Neurological Institute (Phoenix, AZ, USA). The institutional review board (IRB) protocols were approved by the review board in Tianjin General Hospital and Barrow Neurological Institute. Among the eight cases studied, five cases were from the perihematomal tissues of ICH patients who underwent surgical evacuation of hematoma within 24 h of onset at Tianjin General Hospital. The other three cases were from individuals who died from non-neurological diseases and used as controls, which were collected within 4 h after death. Subjects of non-neurological controls had no history of neurological or neuropsychiatric diseases, which was confirmed by histopathological examination.

### Mice

All animal experiments were approved by the Committee on the Ethics of Animal Experiments of

Tianjin Neurological Institute (Tianjin, China) and Barrow Neurological Institute (Phoenix, AZ, USA), and were performed in accordance with the National Institutes of Health Guide for the Care and Use of Laboratory Animals in China and Guide for the Care and Use of Laboratory Animals in USA. Eight to ten week old C57BL/6 male mice were used in this study. All mice were housed in pathogen-free conditions at the animal facilities at Tianjin Neurological Institute or Barrow Neurological Institute. All surgeries were performed under anesthesia. Reporting of this study complies with the ARRIVE (Animal Research: Reporting in vivo Experiments) guidelines (<https://www.nc3rs.org.uk/arrive-guidelines>).<sup>23,24</sup>

### Administration of PLX3397

PLX3397 (Selleckchem, Houston, TX) was dissolved in dimethyl sulfoxide followed by dilution with phosphate-buffered saline (PBS). As previously described,<sup>25,26</sup> mice received daily treatment with vehicle PBS or PLX3397 (40 mg/kg) by oral gavage for 21 days prior to ICH induction. The treatment was continued until the end of experiments.

### ICH induction

Mice were anesthetized with an intraperitoneal injection of ketamine (100 mg/kg) and xylazine (10 mg/kg). Thereafter, mice were placed in a stereotactic frame and a 1 mm hole in diameter was drilled on the right side of skull (2.3 mm lateral to midline, 0.5 mm anterior to bregma). We injected mice using an infusion pump (Kd Scientific Inc., Holliston, MA) in the right striatum with 0.0375U bacterial collagenase (Type IV-S, Sigma, St. Louis, MO) in 0.5  $\mu$ l saline at a rate of 1  $\mu$ l/min at a depth of 3.7 mm beneath the skull, as previously described.<sup>12,27</sup> In some experiments, ICH was also induced by injection of autologous blood using a double-injection method as in our and other's previous publication.<sup>28,29</sup> Thirty microliters of non-heparinized autologous blood was withdrawn from the angular vein and infused as described. The first 5  $\mu$ l was injected at a rate of 1  $\mu$ l/min at a depth of 3 mm beneath the hole to generate a clot after which the needle was moved to a depth of 3.7 mm and paused for 5 min. The remaining 25  $\mu$ l was injected at the same rate of 1  $\mu$ l/min. Sham controls were injected with an equal volume of saline. During surgery, body temperature was maintained at 37°C  $\pm$  0.5°C. The skull hole was closed with bone wax and the incision was closed with sutures following surgery. To avoid dehydration, 0.5 ml of saline (0.9% NaCl) was given to each mouse by s.c. injection immediately after surgery, before being placed in a cage with free access to food and

water. These two procedures of ICH induction resulted in reproducible lesions mostly restricted to the striatum.

### Neurological deficit and brain water content assessment

Neurological tests were performed at days 1 and 3 after ICH by at least two investigators blind to PLX3397 treatment. The modified Neurological Severity Score (mNSS) and corner turning test were performed as previously described.<sup>30,31</sup> The mNSS rates neurological functioning on a scale of 15 and includes a composite of motor, sensory, reflex, and balance tests. The mouse was given one point for the inability to perform each test while deducting one point for the lack of a tested reflex. Finally, an overall score was given to determine impairment in each mouse. The corner turning test was used to assess sensorimotor and postural asymmetries, the tested mouse was allowed to go into a corner with an angle of 30 degrees and was required to turn either to the left or the right to exit the corner. This was repeated and recorded for 10 times, with at least 30 s between trials, and the percentage of right turns in total turns was calculated in this study.

For brain water content assessment, after euthanasia and decapitation at day 3 after ICH, brains were placed into a brain-cutting matrix. Brains were immediately divided into three parts: left hemisphere, right hemisphere, and cerebellum. The tissues were then weighed to obtain the wet weight, followed by drying for 24 h at 100°C to obtain the dry weight. Brain water content was calculated using the following formula:  $(\text{Wet Weight} - \text{Dry Weight}) / \text{Wet Weight} \times 100\%$ .

### Neuroimaging

To detect reactive oxygen species (ROS) generation in the mouse brain after ICH, live bioluminescence images were captured using a Xenogen IVIS200 imager (Caliper LifeSciences, Hopkinton, MA) after i.p. injection of 200 mg/kg Luminol (Invitrogen).<sup>32,33</sup> Signal intensities from the brain were defined and measured in the efficiency mode with the Xenogen system. Data were collected as photons per second per cm<sup>2</sup> using Living Image software (Caliper Life Sciences, Hopkinton, MA).

Magnetic resonance imaging (MRI) was performed using a 7T small-animal MRI, 30-cm horizontal-bore magnet, and BioSpec Avance III spectrometer (Bruker Daltonics Inc., Billerica, MA), which has a 116-mm high-power gradient set (600 mT/m) and a 72-mm whole-body mouse transmit/surface receive coil configuration.

The T2-weighted images (T2) were obtained using the following parameters: repetition time (TR)=4500 ms,

echo time (TE)=65.5 ms, field of view (FOV)=28 × 28 mm<sup>2</sup>, image matrix = 256 × 256, 0.5-mm slice thickness, total 40 scanned slices. Susceptibility weighted imaging (SWI) measurements used a three-dimensional gradient-echo sequence that is sensitive to the presence of paramagnetic substances such as iron compounds. SWI data were acquired with TR 30 ms and TE 10 ms, flip angle = 25°, FOV = 32 × 32 × 16 mm<sup>3</sup>, image matrix = 256 × 256. ICH lesion volumes were determined on T2 and hematoma volumes were determined on SWI with the use of MIPAV software (Supplemental Fig. 1A). The lesion and hematoma volumes were evaluated by at least two blinded investigators. The lesion and hematoma were traced manually on each slice. The areas were then summed and multiplied by the slice thickness. Perihematomal edema volumes were calculated as total lesion volume minus the hematoma volume.

The T1 post-contrast images were recorded after administration of the contrast agent to assess the change in BBB permeability (Supplemental Fig. 1B). Images were acquired with TR=322 ms and TE=10.5 ms, FOV=28 mm, image matrix = 256 × 256, 0.5-mm slice thickness. The post-contrast T1 was obtained 10 min after the administration of gadopentate dimeglumine (Gd-DTPA) (Magnevist, Schering AG, Berlin, Germany) with dosage of 0.2 mmol/kg bodyweight. MRI data were analyzed using the MED × 3.4.3 software package (Medical Numerics Inc, Germantown, MA) on a LINUX workstation. Subtraction maps were obtained by subtracting the pre-contrast T1 images from the post-contrast T1 images. Through this process of imaging and measurement methods, mixed signals stemming from necrotic tissue or coagulated blood were removed. Estimates of the permeability index expressed as rT1, a ratio of the mean signal intensity of a region of interest on the infarction to that of the contralateral homologous normal brain area, were produced using the subtraction maps.<sup>34</sup>

### Histology stains

Immunofluorescence staining was performed as we previously described.<sup>32,33,35</sup> Mice were perfused with PBS followed by 4% paraformaldehyde (PFA). Brains were removed and embedded in paraffin. Five-micrometer thick coronal sections were deparaffinized and rehydrated in a series of ethanol dilutions. Sections were permeabilized and incubated with a blocking solution consisting of 5% goat serum or 5% donkey serum, followed by incubating with antibodies against Iba1 (Wako, Richmond, VA), IL-6 (Santa Cruz Biotechnology, Paso Robles, CA), IL-1β (Santa Cruz Biotechnology, Paso Robles, CA), CD31 (Invitrogen,

Carlsbad, CA), or Claudin5 (Invitrogen, Carlsbad, CA) at 4°C overnight. After washing with PBS, slices were incubated with appropriate fluorochrome conjugated secondary antibodies: donkey anti-rabbit 488 (Invitrogen, Carlsbad, CA), donkey anti-mouse 594 (Invitrogen, Carlsbad, CA), and goat anti-rat 555 (Invitrogen, Carlsbad, CA), respectively, at room temperature for 1 h. Finally, all the slices were incubated with fluoro-shield mounting medium with DAPI (Abcam, Cambridge, MA). Images were taken with a fluorescence microscope (Model BX-61, Olympus, Center Valley, PA). The intensity of immunofluorescence was quantified by using ImageJ (U.S. National Institutes of Health, Washington, DC).

Cresyl violet (Sigma, St. Louis, MO) for neurons and luxol fast blue (Fisher Scientific, Allentown, PA) for myelin staining was performed as previously described.<sup>36</sup> After MRI scanning, the brain was fixed in 4% PFA and dehydrated with 30% sucrose for 2 days at 4°C. Fifty-micrometer-thick cryostat brain sections with a 200 µm interval in the lesion area from each mouse were stained with luxol fast blue and cresyl violet. Injury size was analyzed blindly on each section by two neuroradiologists using ImageJ. A total injury volume was calculated by summation of the volumes on all the sections and then multiplied by the interval.

### Flow cytometry

Flow cytometry was performed to analyze immune cell infiltration and microglia cytokine expression. Briefly, the brain was removed after perfusion with cold PBS and mechanically cut into small pieces using sharp scissors. In all, 1 mg/ml collagenase (Sigma, St. Louis, MO) in 10 mM Hepes/NaOH buffer solution was used to digest the brain tissue at 37°C for 1 h. Cell pellets were collected by centrifugation at 1500 rpm for 5 min, then re-suspended in 70% percoll (Sigma, St. Louis, MO) and 30% percoll was overlaid on top. The gradient was centrifuged at 2000 rpm for 30 min at RT without brake. The monolayer between the interface of 30/70% percoll was harvested as mononuclear cells. Single cells suspensions were stained with antibodies or isotype controls. All antibodies were purchased from BD Bioscience, Inc (San Jose, CA) or eBioscience, Inc (San Diego, CA), unless otherwise indicated. The procedure of cell staining followed the manual protocol. The following antibodies were used: CD3 (145-2C11), NK1.1 (PK136), CD8 (53-6.72), CD45 (30-F11), CD11b (M1/70), CD4 (GK1.4), F4/80 (6F12), Ly6G (1A8), IL-1β (B122), IL-6 (MQ2-6A3), CD19 (1D3). Flow cytometric data were acquired on a FACSAria flow cytometer (BD Biosciences, San Jose, CA) and analyzed with Flow Jo software version 7.6.1 (Informer Technologies, Walnut, CA).

### Western blot

Brain tissues were homogenized and lysed in RIPA buffer (Sigma, St. Louis, MO, USA) supplement with 1 mmol/L phenylmethanesulfonyl fluoride (PMSF) (Sigma, St. Louis, MO, USA). The supernatant was harvested for protein analysis after centrifugation. Proteins were resolved by 10% SDS-PAGE and transferred to a PVDF membrane (Millipore, Billerica, MA, USA). The membrane was blocked with 5% nonfat milk solution for 1 h at room temperature, then incubated with primary antibodies against anti-claudin-5 (1:1000, Invitrogen, Grand Island, NY, USA) and anti-β-actin (1:1000, Cell Signaling Technology, Danvers, MA, USA) overnight at 4°C. After washing, the membrane was incubated with HRP-conjugated rat anti-mouse and goat anti-rabbit secondary antibodies (1:4000; Zymed, Carlsbad, CA, USA) for 1 h at room temperature. Immunoactive bands were detected and captured using a gel imaging system (Bio-Rad, Hercules, CA, USA). The intensity of each band was quantified by the Quantity One software (Bio-Rad, Hercules, CA, USA).

### ELISA

Inflammatory cytokines in brain tissues were analyzed with the enzyme-linked immunosorbent assay (ELISA). Brain homogenates were prepared from ICH mice with or without treatment of PLX3397 at day 3 after ICH. After the total protein concentration was adjusted to 1 mg/mL, cytokine levels in these samples were detected using a Mouse Inflammatory Cytokines Multi-Analyte ELISArray Kit (SABioscience, Valencia, CA) according to the manufacturer's instructions, as previously described.<sup>33</sup>

### Statistical methods

All values are expressed as mean ± SEM. Statistical data analyses were performed using Graphpad 5.0 software. Two-tailed unpaired students *t*-test was used to determine significance of two groups. One-way ANOVA followed by Tukey post hoc test or by two-way ANOVA with multiple comparisons were used for comparison of multi-group data. Values of *p* < 0.05 were considered significant.

## Results

### Microglial activation and production of inflammation mediators after ICH in humans and mice

Cells expressing the microglial marker Iba-1 were populated in the perihematomal brain sections from patients

within 24 h after ICH (Figure 1(a)). Differing from the healthy controls, microglia in ICH patients had larger size with thick proximal processes (Figure 1(a)), together with the up-regulation of inflammatory mediators such as IL-1 $\beta$  and IL-6 (Figure 1(a) and (b)).

Next, we examined microglia expressing IL-6 or IL-1 $\beta$  in ICH mice induced by injection of collagenase. At day 1 after ICH, flow cytometry analysis shows increased percentage of IL-6- or IL-1 $\beta$ -expressing cells in microglia isolated and gated as the CD11b<sup>+</sup>CD45<sup>int</sup> subset (Figure 1(c) and (d)). These data indicate early activation of microglia and their expression of inflammatory mediators following ICH.

### CSF1R inhibition eliminates microglia in the brain after ICH

As shown in Figure 2(a), mice were treated with vehicle PBS or PLX3397 for consecutive 21 days prior to ICH induction. Treatment was sustained until the end of experiments. At day 3 after ICH induced by injection of collagenase, the efficacy of microglia elimination by PLX3397 treatment was determined using flow cytometry (Figure 2(b) and (c)). We found that ~90% of microglia (CD11b<sup>+</sup>CD45<sup>int</sup>) cells were depleted in mice subjected to PLX3397 treatment before or after ICH (Figure 2(b) and (c)). In contrast, the number of

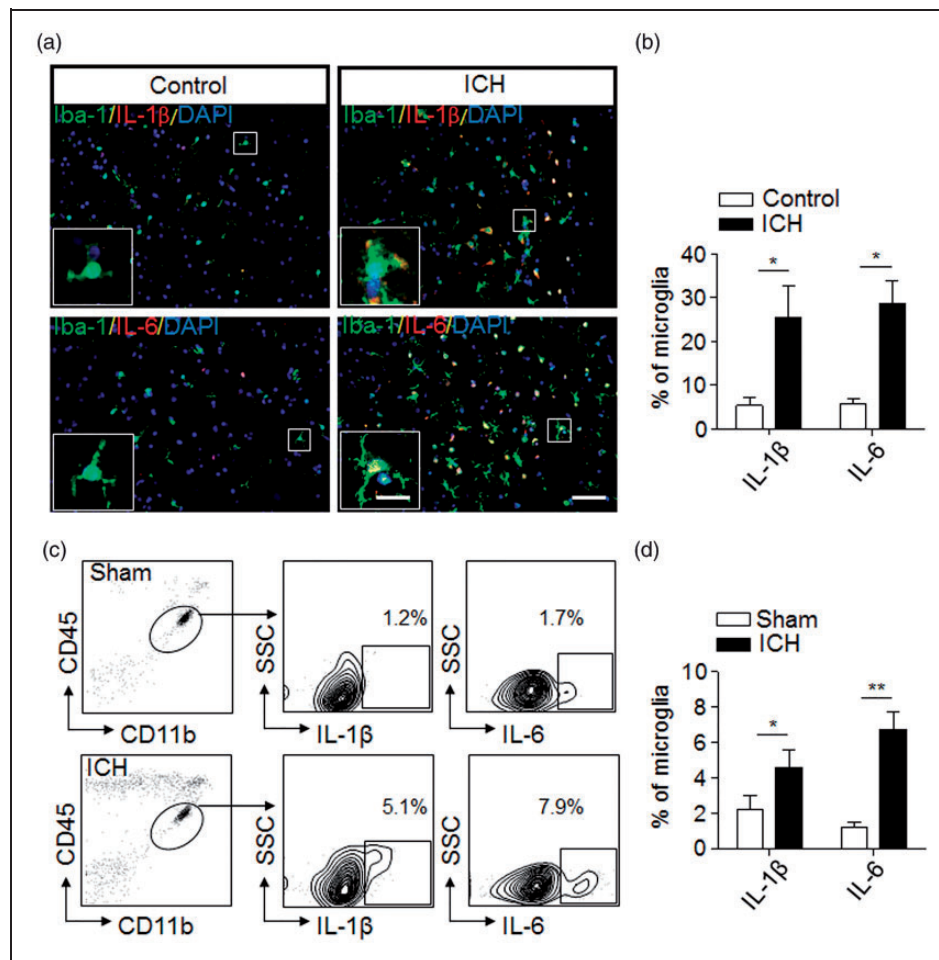


**Figure 1.** Microglial activation and production of inflammation mediators after ICH. (a) Immunostaining of brain sections from ICH patients or non-neurological disease controls shows Iba-1<sup>+</sup> cells (green) expressing interleukin-1 beta (IL-1 $\beta$ ) (red) and IL-6 (red). Scale bar: 50  $\mu$ m; insert: 20  $\mu$ m. (b) Quantification of microglia expressing IL-1 $\beta$  and IL-6 in the brain section from non-neurological disease controls and patients with ICH.  $n = 20$  sections from five ICH patients,  $n = 15$  sections from three non-neurological controls in three independent experiments. Mean  $\pm$  s.e.m. \* $p < 0.05$ . (c,d) Expression of IL-1 $\beta$  and IL-6 in microglia (CD11b<sup>+</sup>CD45<sup>int</sup>) from sham control and ICH mice induced by injection of collagenase (0.0375U). Single cell suspensions were prepared from mouse brain tissues at 24 h after ICH or sham procedures. ICH was induced by collagenase injection. Quantification of microglia expressing IL-1 $\beta$  or IL-6 were determined by flow cytometry (c). Summarized results from three independent experiments are shown in (d). Mean  $\pm$  s.e.m.  $n = 6$  mice per group, \* $p < 0.05$ ; \*\* $p < 0.01$ .

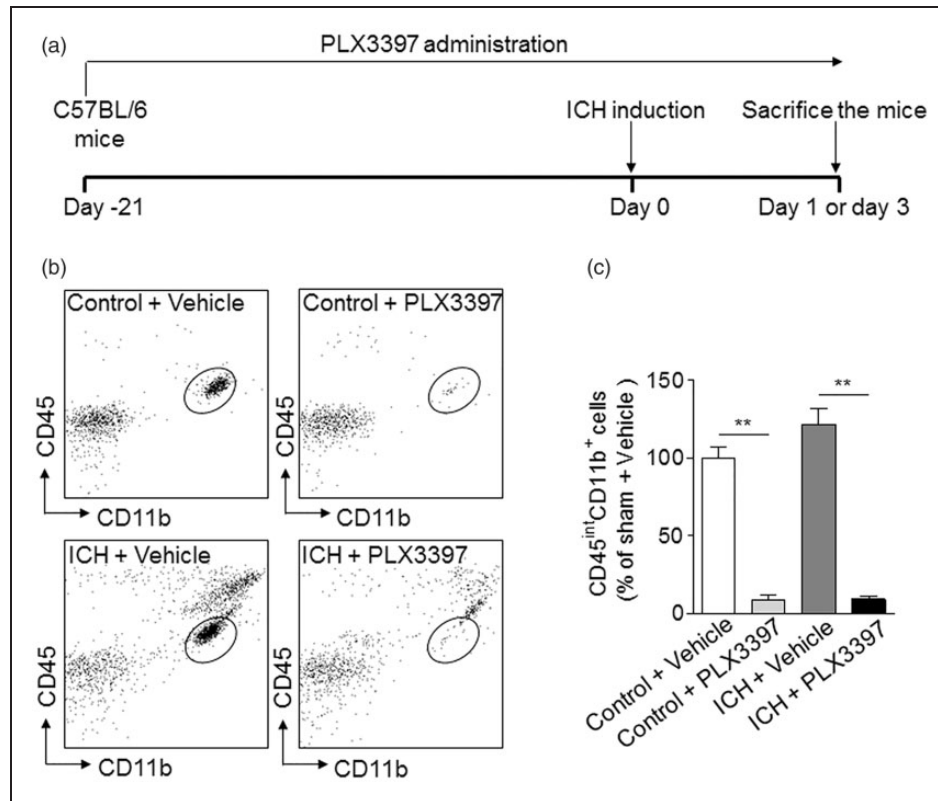


**Figure 2.** CSF1R inhibition eliminates microglia in brain. (a) Schematics of microglia depletion and experimental design. Mice were treated with 40 mg/kg body weight PLX3397 for 21 days before ICH induction and continued until the end of experiments. (b,c) After PLX3397 treatment for 21 days, ICH was induced by injection of 0.0375U collagenase. After ICH, treatment was continued until mice were sacrificed. At day 3 after ICH, the number of brain microglia (CD45<sup>int</sup>CD11b<sup>+</sup>) was analyzed by flow cytometry in the following groups of mice: ICH and non-ICH control mice receiving PLX3397 or vehicle. Gating strategy (b) and summarized results from two independent experiments (c) are shown. Mean  $\pm$  s.e.m.  $n = 6$  mice per group, \*\* $p < 0.01$ .

monocytes or macrophages in the spleen were not significantly altered after PLX3397 treatment for 21 days and Iba-1<sup>+</sup> cells in the brain are not CD169<sup>+</sup> cells in control mice receiving vehicle (CD169 is a specific marker of monocytes and can be used to distinguish microglia from infiltrating myeloid cells, data not shown).<sup>37,38</sup> These data demonstrate the efficacy of microglia depletion using PLX3397 and show that the dependence of CSF1R for microglia survival is independent of ICH activation.

#### CSF1R inhibition attenuates neurodeficits and brain edema after ICH

To determine the impact of CSF1R inhibition and microglia depletion on brain injury after ICH, we examined neurodeficits, lesion volume, perihematomal edema, and brain water content in ICH mice receiving PLX3397 or vehicle controls. Neurodeficits were assessed using a mNSS and corner turning test. Brain edema and hemorrhage volume were evaluated with T2 and SWI MRI images at day 3 after ICH in both

models (Supplemental Fig. 1A). Brain water content was measured using the wet/dry weight method. We found that PLX3397 reduced neurodeficits, lesion volume, perihematomal edema, and brain water content after ICH induced by injection of collagenase or autologous blood (Figure 3(a)–(f)).

#### The benefit of CSF1R inhibition is independent of lesion size or hematoma volume

The clinical heterogeneity of stroke results in various brain lesion sizes that may determine the extent of microglial activation and brain inflammation after stroke.<sup>39</sup> To determine whether the protection conferred by CSF1R inhibition can be affected by lesion size after ICH, we induced ICH by injection of different volumes of collagenase (0.01, 0.03, and 0.05 U) to produce different hemorrhagic injury volumes. PLX3397 reduced neurodeficits, lesion volume, and perihematomal edema in ICH mice receiving different volumes of collagenase (Figure 4(a)–(e)). These results suggest that microglia may significantly contribute to brain injury

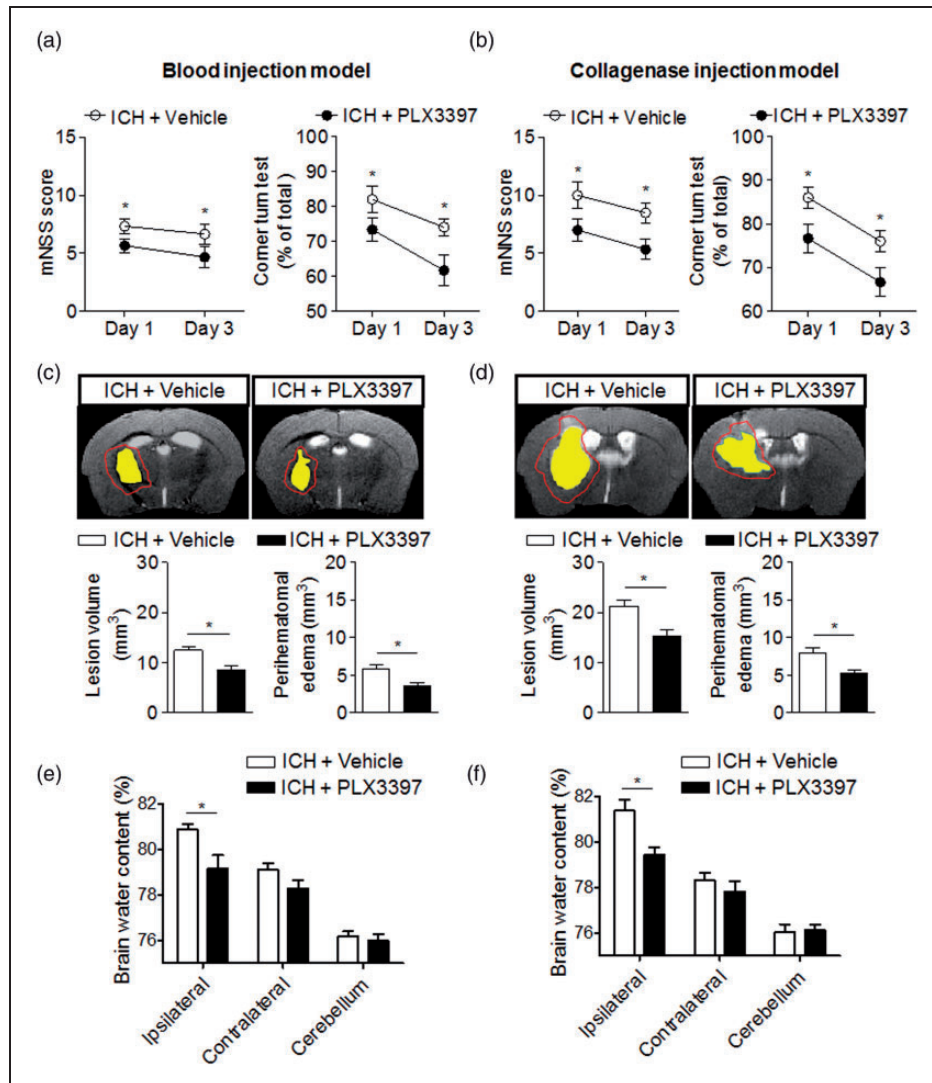


**Figure 3.** CSF1R inhibition attenuates neurodeficits and brain edema in two mouse models of ICH. (a–f) PLX3397 reduced neurodeficits, lesion volume, and perihematomal edema volume after ICH. Representative 7T MRI images and quantification of lesion volume and perihematomal edema volume in ICH mice receiving PLX3397 treatment versus untreated controls. ICH was induced by injection of autologous blood (a) or collagenase (b), mice treated with PLX3397 had reduced neurodeficits than untreated controls at indicated time points after ICH induced by injection of autologous blood (a) and collagenase (b). Multi-modal 7T MRI were performed to visualize lesion (T2) and hematoma (SWI). Perihematomal edema volume was calculated by subtracting the hematoma volume from lesion volume. Red lines delineate lesion area, yellow shaded regions represent hematoma area. The method used to determine perihematomal edema volume is depicted in Supplemental Fig. 1A. At day 3 after ICH, lesion volume and brain edema were assessed by this method in autologous blood model (c) and collagenase model (d). At day 3 after ICH, PLX3397 treatment decreased brain water content in ipsilateral hemisphere in autologous blood model (e) and collagenase model (f). Mean  $\pm$  s.e.m.  $n = 10$  mice per group from two independent experiments, \* $p < 0.05$ .

even if the initial lesion size is small, implying microglia as an active yet sensitive player in hemorrhagic brain injury.

### CSF1R inhibition reduces brain-infiltrating leukocytes after ICH

In addition to microglial activation, infiltrating leukocytes and their intimate crosstalk with microglia can

contribute to brain inflammation and brain damage after ICH. To determine the impact of CSF1R inhibition and microglia elimination on inflammatory responses, we gated and quantified cellular infiltrates after ICH (Figure 5(a)). At day 1 after ICH, the numbers of CD4<sup>+</sup> T cells (CD45<sup>high</sup> CD3<sup>+</sup>CD4<sup>+</sup>), NK cells (CD45<sup>high</sup>CD3<sup>-</sup>NK1.1<sup>+</sup>), macrophage (CD45<sup>high</sup>CD11b<sup>+</sup>F4/80<sup>+</sup>), and neutrophils (CD45<sup>high</sup>CD11b<sup>+</sup>Ly-6G (1A8)<sup>+</sup>) in the brain were reduced in ICH

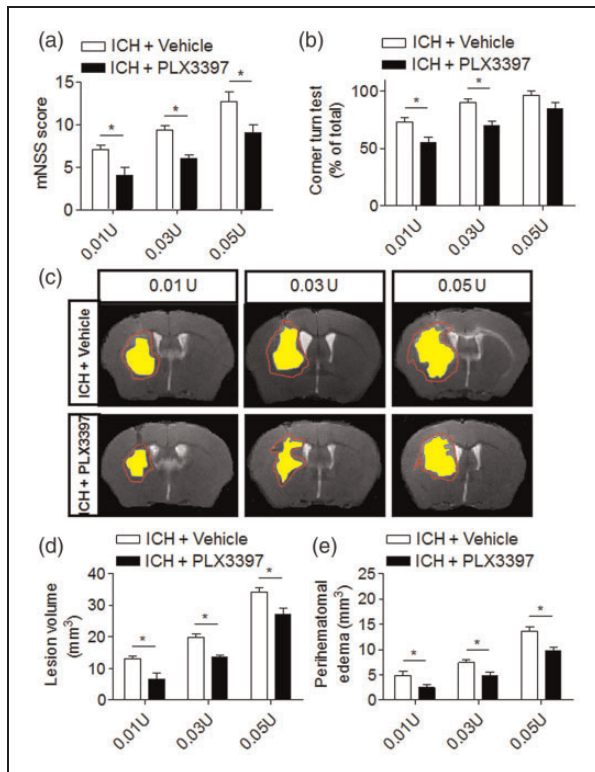


**Figure 4.** The benefit of CSF1R inhibition is independent of hemorrhagic injury volume. ICH was induced by injection of 0.01U, 0.03U, and 0.05U collagenase. Neurological deficits and lesion volume, as well as perihematomal volume were measured at day 3 post-surgery. (a,b) ICH mice treated with PLX3397 had lower mNSS score and better performance in the corner turn test. Mean  $\pm$  s.e.m.  $n = 6$  mice per group, \* $p < 0.05$ . (c–e) PLX3397 treatment reduced lesion volume and perihematomal volume in ICH mice. Red lines delineate lesion volume, yellow shaded areas depict hematoma area. Mean  $\pm$  s.e.m.  $n = 6$  mice per group from two independent experiments, \* $p < 0.05$ .

mice treated with PLX3397 (Figure 5(b)). At day 3 post-ICH, the number of assessed immune cell subsets ( $CD4^+$  T cell,  $CD8^+$  T cell, B cell, NK cell, macrophage, and neutrophil) were all reduced in ICH mice treated with PLX3397 (Figure 5(c)). This result shows that CSF1R inhibition and microglia elimination reduce leukocyte infiltration in the brain after ICH, suggesting a key role for microglia in the enhancement of immune cell homing into the brain.

#### CSF1R inhibition reduced brain inflammation after ICH

ROS are a key factor that activates cell death pathways. We quantified ROS levels using in vivo bioluminescence imaging at day 3 after ICH in collagenase model and found dramatically reduced ROS signals in ICH mice treated with PLX3397 relative to controls

(Figure 6(a) and (b)). To understand the impact of microglial depletion on the expression of inflammatory mediators, we measured the levels of inflammatory cytokines in brain homogenates of ICH mice with or without PLX3397 treatment. Of interest, brain homogenates from ICH mice receiving PLX3397 had lower protein levels of interleukin-1 alpha ( $IL-1\alpha$ ),  $IL-1\beta$ ,  $IL-6$ , interferon gamma ( $IFN-\gamma$ ), and granulocyte-macrophage colony-stimulating factor (GM-CSF) than untreated controls (Figure 6(c)), whereas PLX3397 does not affect the expression of these factors at baseline level before ICH (data not shown). Reportedly, CSF1R inhibition can eliminate microglia without affecting the baseline expression of inflammatory cytokines in the brain.<sup>15</sup> These data indicate that CSF1R inhibition and microglia depletion can reduce brain inflammation after ICH.

#### CSF1R inhibition preserves the integrity of BBB after ICH

BBB dysfunction after ICH can contribute to vasogenic brain edema and perihematomal edema expansion.<sup>1,7</sup> We therefore examined the impact of CSF1R inhibition and microglia depletion on the integrity of the BBB after ICH. The presence of parenchymal enhancement on contrast enhanced T1 is generally accepted as an indicator of contrast medium leakage across the disrupted BBB. We further evaluated the vascular permeability based on the images collected in the ICH models. As in Figure 7(a) and (b), parenchymal enhancement of vehicle group is much higher than in the PLX3397 treated group. Western blot and immunostaining show that PLX3397 preserved a tight junction protein, claudin-5, after ICH (Figure 7(c)–(f)). These results suggest that CSF1R inhibition and microglia depletion can preserve BBB integrity after ICH.

#### Discussion

This study provides novel evidence that microglia exert a detrimental impact on hemorrhagic brain injury. As documented here, microglial elimination by CSF1R inhibition can be sustained after ICH. The depletion of microglia reduces lesion size, brain edema, and neurodeficits in two separate ICH mouse models. The protection conferred by CSF1R inhibition is independent of ICH volume. Importantly, microglial elimination attenuates leukocyte infiltration and inflammatory cytokine levels in the brain after ICH. Moreover, removal of microglia preserves the integrity of the BBB after ICH. In addition to supporting a deleterious role of microglia, these findings show that microglia are critical for the development of inflammatory responses after ICH, suggesting that microglia may be pivotal for

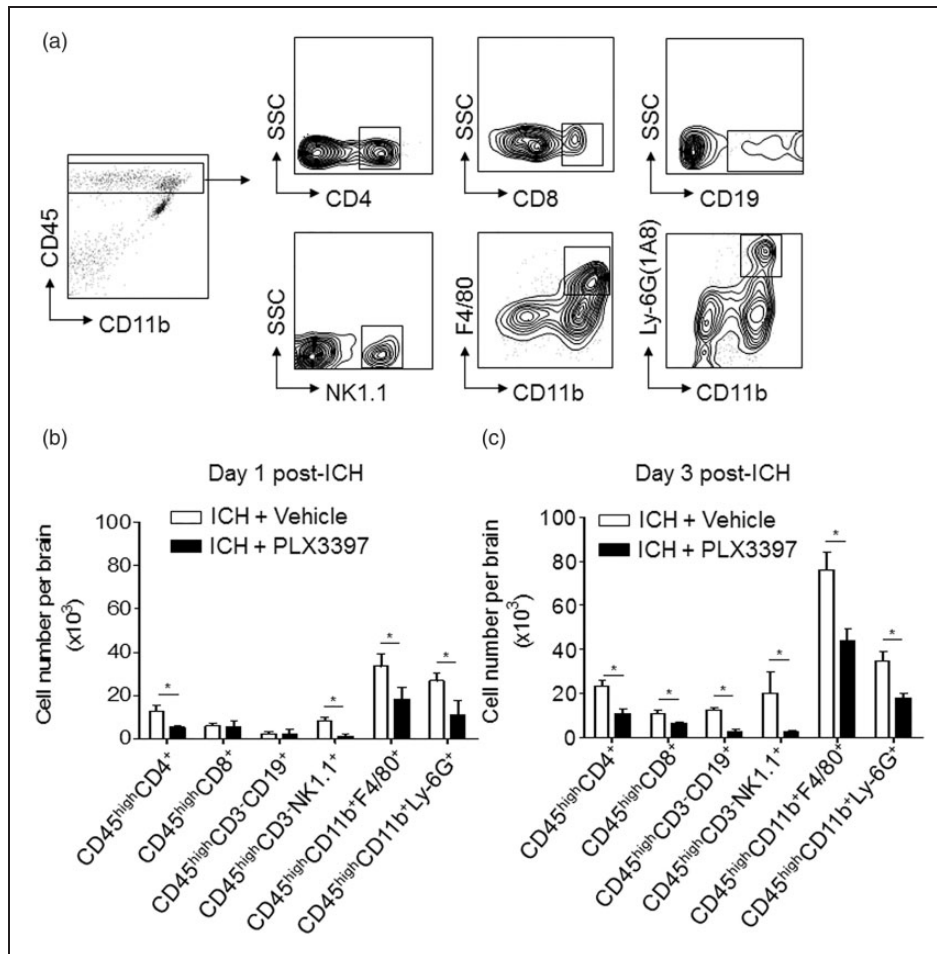


**Figure 5.** CSFIR inhibition reduces brain-infiltrating leukocytes after ICH. ICH was induced by 0.0375U collagenase injection. At day 1 or 3 after ICH, inflammatory cells were isolated from brain tissues of ICH mice treated with PLX3397 or vehicle (control). (a) Gating strategy of brain-infiltrating immune cells including CD4<sup>+</sup>T cell (CD45<sup>high</sup>CD3<sup>+</sup>CD4<sup>+</sup>), CD8<sup>+</sup>T cell (CD45<sup>high</sup>CD3<sup>+</sup>CD8<sup>+</sup>), B cell (CD45<sup>high</sup>CD3<sup>-</sup>CD19<sup>+</sup>), NK cell (CD45<sup>high</sup>CD3<sup>-</sup>NK1.1<sup>+</sup>), macrophage (CD45<sup>high</sup>CD11b<sup>+</sup>F4/80<sup>+</sup>), and neutrophils (CD45<sup>high</sup>CD11b<sup>+</sup>Ly-6G(1A8)<sup>+</sup>). (b,c) Summarized results show declined infiltration of lymphocytes, monocytes, and neutrophils in the brain of ICH mice receiving PLX3397 treatment at day 1 and 3. Mean  $\pm$  s.e.m.  $n = 6$  mice per group from three independent experiments, \* $p < 0.05$ .

neural-immune crosstalk during acute hemorrhagic brain injury.

Evidence suggests that microglial activation occurs very early after ICH.<sup>40</sup> The mixed yet unclear role of microglia in brain injury is suggested by their multiple capabilities of phagocytosis, production of inflammatory or anti-inflammatory cytokines, and antigen presentation.<sup>41,42</sup> Despite previous studies showing that microglial activation correlates with observations of perihematomal edema in ICH and inhibition of microglia activation via minocycline or PPAR- $\gamma$  agonists can provide neuroprotection after ICH,<sup>43,44</sup> no direct evidence is available to understand the precise contribution of microglia to hemorrhagic brain injury. In support of previous findings, we show that depletion of microglia confers protection against ICH in two separate mouse models of ICH, independent of lesion size.

Together with the data showing activation and production of inflammatory mediators by human microglia after ICH, these results allow us to infer a harmful role for microglia and their activation in acute hemorrhagic brain injury.

To determine possible mechanisms by which microglial elimination might confer protection after ICH, we examined the immune responses in the brain. Beyond the production of pro-inflammatory cytokines, ROS, and chemokines, microglia can also enhance early neuroinflammation by recruiting and activating leukocytes to worsen ICH-induced brain injury. Although our data cannot conclude the precise cellular sources of these inflammatory factors after ICH, we show that microglial elimination can reduce a variety of pro-inflammatory factors and ROS production after ICH, accompanied with a decrease of infiltrating leukocytes

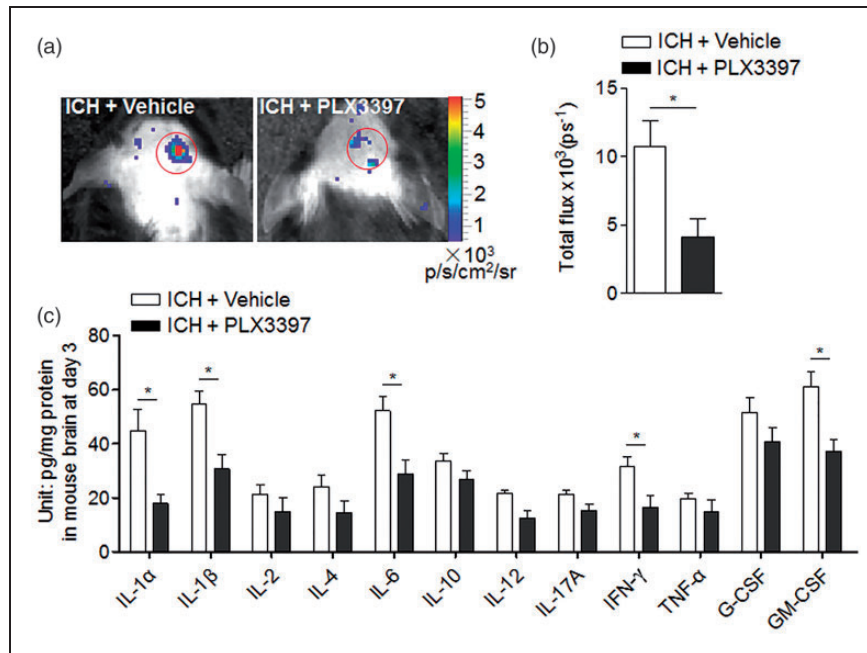


**Figure 6.** CSFIR inhibition reduced brain inflammation after ICH. ICH was induced by injecting 0.0375U collagenase. (a,b) Visualization of ROS generation in vivo bioluminescence imaging and quantification of signal strength in ICH mice receiving PLX3397 and vehicle at day 3 after collagenase model induction. (c) At day 3 after ICH, expression of inflammatory mediators in ICH mice treated with PLX3397 versus untreated controls. Cytokine expression was detected using a Multi-Analyte ELISArray kit. Mean  $\pm$  s.e.m.  $n = 3$  mice per group from two independent experiments, \* $p < 0.05$ .

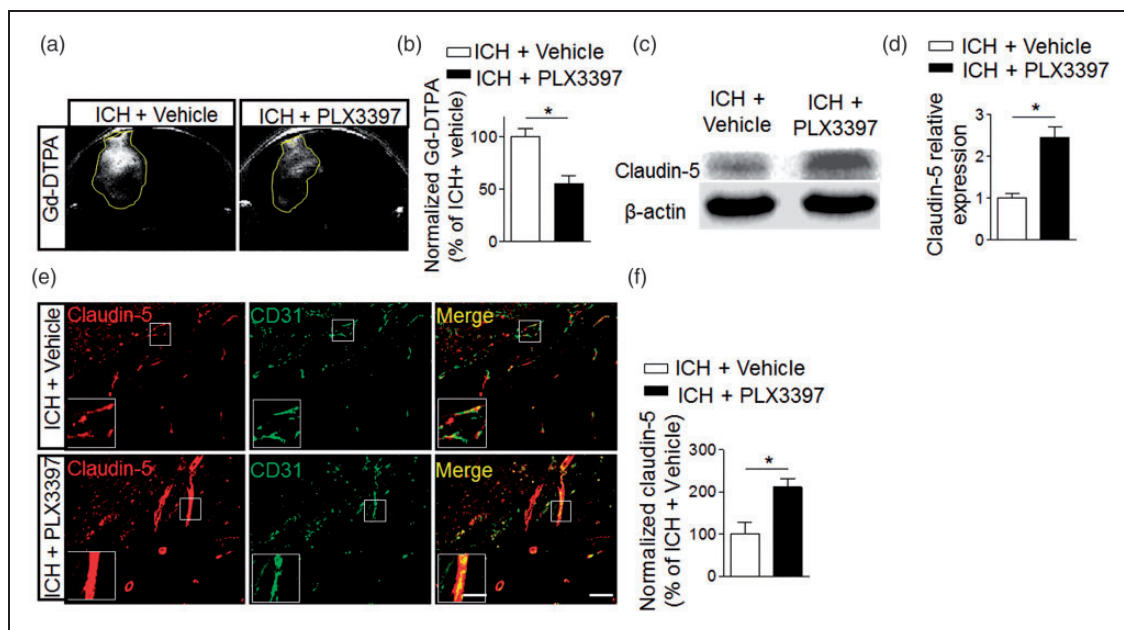


**Figure 7.** CSFIR inhibition preserves the integrity of blood–brain barrier after ICH. ICH was induced by injecting 0.0375U collagenase. (a) MRI was performed to determine the permeability of the blood–brain barrier in ICH mice treated with PLX3397 or vehicle. Images were scanned under T1 sequence before and after injection of Gd-TDPA at day 3 after ICH. Gd-enhancement was calculated as follows:  $rT1\% = (\text{mean signal intensity of a region of the ipsilateral} - \text{mean signal intensity of the contralateral homologous normal brain area}) / \text{mean signal intensity of the contralateral homologous normal brain area}$ . (b) Bar graph shows Gd-enhancement at day 3 after ICH. Mean  $\pm$  s.e.m.  $n = 3$  mice per group from two independent experiments, \* $p < 0.05$ . (c) Western blot was performed to assess the expression of claudin-5 in the ipsilateral hemisphere of ICH mice treated with PLX3397 versus vehicle controls. (d) Bar graph shows higher expression level of claudin-5 in the ipsilateral hemisphere of ICH mice treated with PLX3397.  $n = 6$  mice per group. (e) Brain sections from ICH mice treated with PLX3397 or vehicle were stained with CD31 (green) and claudin-5 (red) at day 3 after ICH. Scale bar: 50  $\mu\text{m}$ ; insert: 20  $\mu\text{m}$ . (f) Summarized results show that ICH mice treated with PLX3397 had reduced claudin-5 loss in immunofluorescence intensity within the lesion area. Mean  $\pm$  s.e.m.  $n = 12$  sections from three mice per group from three independent experiments, \* $p < 0.05$ .

and preserved BBB integrity. Because brain inflammation and BBB dysfunction are critical factors that contribute to vasogenic edema and brain damage after ICH, we postulate that the mitigated brain inflammatory milieu after the removal of microglia contributes to the protection conferred by CSF1R inhibition in ICH. However, the precise operating mechanisms through which microglia interact with infiltrating leukocytes and orchestrate brain inflammatory milieu after ICH require further investigations. The pathological phenotype of brain edema manifests early after injury and is a composite of multiple pathways, including both cellular responses to injury and perturbation of the BBB.<sup>1</sup>

Because CSF1R is also expressed by myeloid cells including monocytes and macrophages besides brain-resident microglia, there is a possibility that PLX3397 may impact the baseline immune responses that contribute to the protection after ICH. However, previous evidence shows that elimination of microglia with PLX3397 had neither detrimental impact on the neurological function nor baseline brain inflammatory status under physiological conditions.<sup>45,46</sup> In agreement with these findings, we found that CSF1R inhibition appears to only affect inflammation status after ICH. In addition, PLX3397 treatment has minimal effect on monocytes and macrophages in the periphery.<sup>15,47–49</sup> These results suggest that protection conferred by PLX3397 treatment is caused by the removal of microglia. To understand this relatively microglia-specific effect, we postulate that in the periphery, macrophage populations can be replenished by circulating monocytes derived from multipotent hematopoietic stem cells.<sup>50,51</sup> Different than the periphery, the brain is separated from circulation by the BBB, and thus there is a possibility that replenishment of microglia is relatively limited in the brain. Another possibility is the vast differences regarding the levels of environmental factors in the CNS vs. periphery and/or the discrepancy of the expressions of receptors on the peripheral myeloid cells vs. brain microglia, which may be responsible for their different susceptibility to CSF1R inhibition. These possibilities require further investigations, albeit other possibilities cannot be excluded.

Our results suggest a detrimental role of microglia during the acute phase. However, still unclear are whether and how microglia may impact brain recovery after ICH. Future studies are required to eliminate microglia after the acute phase of ICH and determine the extent and mechanisms responsible for the potential impact of microglia in brain recovery after ICH.

To conclude, our data reveal that microglia are key elements in the orchestration of brain inflammation after ICH and therefore shed new light on pathogenesis of ICH.

## Funding

The author(s) disclosed receipt of the following financial support for the research, authorship, and/or publication of this article: National Basic Research Program of China grant 2013CB966900; National Science Foundation of China grants 81230028, 81301044, and 81471535; US National Institutes of Health grants R01NS092713; American Heart Association grant 16SDG27250236; and National Multiple Sclerosis Society research grant RG-1507-05318.

## Acknowledgements

The authors thank Y Fu for technical assistance.

## Declaration of conflicting interests

The author(s) declared no potential conflicts of interest with respect to the research, authorship, and/or publication of this article.

## Authors' contributions

F.-D.S., K.S., and Q.L. formulated the study concept and wrote the paper. M.L., Z.L., H.R., and W.-N.J. performed experiments. M.L., Z.L., and K.W. analyzed the data, interpreted the results, and assisted preparation of the manuscript.

## Supplementary material

Supplementary material for this paper can be found at <http://jcbfm.sagepub.com/content/by/supplemental-data>

## References

1. Urday S, Kimberly WT, Beslow LA, et al. Targeting secondary injury in intracerebral haemorrhage-perihaematoma oedema. *Nat Rev Neurol* 2015; 11: 111–122.
2. Iadecola C and Anrather J. The immunology of stroke: from mechanisms to translation. *Nat Med* 2011; 17: 796–808.
3. Macrez R, Ali C, Toutirais O, et al. Stroke and the immune system: from pathophysiology to new therapeutic strategies. *Lancet Neurol* 2011; 10: 471–480.
4. Wang J. Preclinical and clinical research on inflammation after intracerebral hemorrhage. *Prog Neurobiol* 2010; 92: 463–477.
5. Chamorro A, Meisel A, Planas AM, et al. The immunology of acute stroke. *Nat Rev Neurol* 2012; 8: 401–410.
6. Fu Y, Liu Q, Anrather J, et al. Immune interventions in stroke. *Nat Rev Neurol* 2015; 11: 524–535.
7. Keep RF, Hua Y and Xi G. Intracerebral haemorrhage: mechanisms of injury and therapeutic targets. *Lancet Neurol* 2012; 11: 720–731.
8. Mracsko E and Veltkamp R. Neuroinflammation after intracerebral hemorrhage. *Front Cell Neurosci* 2014; 8: 388.
9. Taylor RA and Sansing LH. Microglial responses after ischemic stroke and intracerebral hemorrhage. *Clin Dev Immunol* 2013; 2013: 746068.
10. Wang YC, Zhou Y, Fang H, et al. Toll-like receptor 2/4 heterodimer mediates inflammatory injury in intracerebral hemorrhage. *Ann Neurol* 2014; 75: 876–889.

11. Wu J, Yang S, Xi G, et al. Microglial activation and brain injury after intracerebral hemorrhage. *Acta Neurochirurg Suppl* 2008; 105: 59–65.
12. Wang J, Rogove AD, Tsirka AE, et al. Protective role of tuftsin fragment 1-3 in an animal model of intracerebral hemorrhage. *Ann Neurol* 2003; 54: 655–664.
13. Hu X, Leak RK, Shi Y, et al. Microglial and macrophage polarization-new prospects for brain repair. *Nat Rev Neurol* 2015; 11: 56–64.
14. Ponomarev ED, Maresz K, Tan Y, et al. CNS-derived interleukin-4 is essential for the regulation of auto-immune inflammation and induces a state of alternative activation in microglial cells. *J Neurosci* 2007; 27: 10714–10721.
15. Elmore MR, Najafi AR, Koike MA, et al. Colony-stimulating factor 1 receptor signaling is necessary for microglia viability, unmasking a microglia progenitor cell in the adult brain. *Neuron* 2014; 82: 380–397.
16. Dagher NN, Najafi AR, Kayala KM, et al. Colony-stimulating factor 1 receptor inhibition prevents microglial plaque association and improves cognition in 3xTg-AD mice. *J Neuroinflamm* 2015; 12: 139.
17. Patel S and Player MR. Colony-stimulating factor-1 receptor inhibitors for the treatment of cancer and inflammatory disease. *Curr Top Med Chem* 2009; 9: 599–610.
18. Erblich B, Zhu L, Etgen AM, et al. Absence of colony stimulation factor-1 receptor results in loss of microglia, disrupted brain development and olfactory deficits. *PLoS One* 2011; 6: e26317.
19. Nandi S, Gokhan S, Dai XM, et al. The CSF-1 receptor ligands IL-34 and CSF-1 exhibit distinct developmental brain expression patterns and regulate neural progenitor cell maintenance and maturation. *Dev Biol* 2012; 367: 100–113.
20. Li J, Chen K, Zhu L, et al. Conditional deletion of the colony stimulating factor-1 receptor (c-fms proto-oncogene) in mice. *Genesis* 2006; 44: 328–335.
21. Lin H, Lee E, Hestir K, et al. Discovery of a cytokine and its receptor by functional screening of the extracellular proteome. *Science* 2008; 320: 807–811.
22. Elmore MR, Lee RJ, West BL, et al. Characterizing newly repopulated microglia in the adult mouse: impacts on animal behavior, cell morphology, and neuroinflammation. *PLoS One* 2015; 10: e0122912.
23. Kilkenny C, Browne WJ, Cuthill IC, et al. Improving bioscience research reporting: the ARRIVE guidelines for reporting animal research. *PLoS Biol* 2010; 8: e1000412.
24. Schulz KF, Altman DG, Moher D, et al. CONSORT 2010 statement: updated guidelines for reporting parallel group randomised trials. *BMJ* 2010; 340: c332.
25. Stafford JH, Hirai T, Deng L, et al. Colony stimulating factor 1 receptor inhibition delays recurrence of glioblastoma after radiation by altering myeloid cell recruitment and polarization. *Neuro Oncol* 2016; 18: 797–806.
26. Escamilla J, Schokrpur S, Liu C, et al. CSF1 receptor targeting in prostate cancer reverses macrophage-mediated resistance to androgen blockade therapy. *Cancer Res* 2015; 75: 950–962.
27. Grossetete M and Rosenberg GA. Matrix metalloproteinase inhibition facilitates cell death in intracerebral hemorrhage in mouse. *J Cerebr Blood Flow Metab* 2008; 28: 752–763.
28. Rynkowski MA, Kim GH, Komotar RJ, et al. A mouse model of intracerebral hemorrhage using autologous blood infusion. *Nat Protocols* 2008; 3: 122–128.
29. Sun N, Shen Y, Han W, et al. Selective sphingosine-1-phosphate receptor 1 modulation attenuates experimental intracerebral hemorrhage. *Stroke* 2016; 47: 1899–906.
30. Hua Y, Schallert T, Keep RF, et al. Behavioral tests after intracerebral hemorrhage in the rat. *Stroke* 2002; 33: 2478–2484.
31. Chen J, Sanberg PR, Li Y, et al. Intravenous administration of human umbilical cord blood reduces behavioral deficits after stroke in rats. *Stroke* 2001; 32: 2682–2688.
32. Gan Y, Liu Q, Wu W, et al. Ischemic neurons recruit natural killer cells that accelerate brain infarction. *Proc Natl Acad Sci USA* 2014; 111: 2704–2709.
33. Hao J, Liu R, Piao W, et al. Central nervous system (CNS)-resident natural killer cells suppress Th17 responses and CNS autoimmune pathology. *J Exp Med* 2010; 207: 1907–1921.
34. Li YJ, Chang GQ, Liu Y, et al. Fingolimod alters inflammatory mediators and vascular permeability in intracerebral hemorrhage. *Neurosci Bull* 2015; 31: 755–762.
35. Liu Q, Sanai N, Jin WN, et al. Neural stem cells sustain natural killer cells that dictate recovery from brain inflammation. *Nat Neurosci* 2016; 19: 243–252.
36. Li M, Akhavan-Sharif RM, Friedlander RM, et al. What sequences on high-field MR best depict temporal resolution of experimental ICH and edema formation in mice? *J Biomed Biotechnol* 2012; 2012: 961461.
37. Butovsky O, Siddiqui S, Gabriely G, et al. Modulating inflammatory monocytes with a unique microRNA gene signature ameliorates murine ALS. *J Clin Invest* 2012; 122: 3063–3087.
38. Gao L, Brenner D, Llorens-Bobadilla E, et al. Infiltration of circulating myeloid cells through CD95L contributes to neurodegeneration in mice. *J Exp Med* 2015; 212: 469–480.
39. MacLellan CL, Silasi G, Auriat AM, et al. Rodent models of intracerebral hemorrhage. *Stroke* 2010; 41(10 Suppl): S95–S98.
40. Wang J and Dore S. Inflammation after intracerebral hemorrhage. *J Cerebr Blood Flow Metab* 2007; 27: 894–908.
41. Wang J and Tsirka SE. Contribution of extracellular proteolysis and microglia to intracerebral hemorrhage. *Neurocrit Care* 2005; 3: 77–85.
42. Stoll G, Schroeter M, Jander S, et al. Lesion-associated expression of transforming growth factor-beta-2 in the rat nervous system: evidence for down-regulating the phagocytic activity of microglia and macrophages. *Brain Pathol* 2004; 14: 51–58.
43. Zhao X, Sun G, Zhang J, et al. Hematoma resolution as a target for intracerebral hemorrhage treatment: role for peroxisome proliferator-activated receptor gamma in microglia/macrophages. *Ann Neurol* 2007; 61: 352–362.

44. Zhao F, Hua Y, He Y, et al. Minocycline-induced attenuation of iron overload and brain injury after experimental intracerebral hemorrhage. *Stroke* 2011; 42: 3587–3593.
45. Sherr CJ, Rettenmier CW, Sacca R, et al. The c-fms proto-oncogene product is related to the receptor for the mononuclear phagocyte growth factor, CSF-1. *Cell* 1985; 41: 665–676.
46. Luo J, Elwood F, Britschgi M, et al. Colony-stimulating factor 1 receptor (CSF1R) signaling in injured neurons facilitates protection and survival. *J Exp Med* 2013; 210: 157–172.
47. Mok S, Koya RC, Tsui C, et al. Inhibition of CSF-1 receptor improves the antitumor efficacy of adoptive cell transfer immunotherapy. *Cancer Res* 2014; 74: 153–161.
48. Mok S, Tsoi J, Koya RC, et al. Inhibition of colony stimulating factor-1 receptor improves antitumor efficacy of BRAF inhibition. *BMC Cancer* 2015; 15: 356.
49. Abou-Khalil R, Yang F, Mortreux M, et al. Delayed bone regeneration is linked to chronic inflammation in murine muscular dystrophy. *J Bone Mineral Res* 2014; 29: 304–315.
50. Hashimoto D, Chow A, Noizat C, et al. Tissue-resident macrophages self-maintain locally throughout adult life with minimal contribution from circulating monocytes. *Immunity* 2013; 38: 792–804.
51. Sieweke MH and Allen JE. Beyond stem cells: self-renewal of differentiated macrophages. *Science* 2013; 342: 1242974.